日本原子力研究所
シビアアクシデント研究ワークショップ(SARJ－99)
1999年11月8－10日，東京

AXISYMMETRIC GLOBAL STRUCTURAL ANALYSIS OF PRESTRESSED CONCRETE CONTAINMENT VESSEL BEYOND DESIGN PRESSURE

Takako Kashiwase
Systems Safety Department
Nuclear Pow er Engineering Corporation
Tel:+81(3)3435-3402 Fax:+81(3)3435-3411
Kashiw ase@nupec.or.jp

Masahito Sato
Lattice Co., Ltd.
Tel:+81(3)5416-8242 Fax:+81(3)5476-8244
sato@lattice-inc.co.jp

ABSTRACT

NUPEC has been planning the ultimate strength test of PCCV imaging severe accident, in cooperation with USNRC. The test model is 1/4 uniform scale model of Japan actual PCCV in which design pressure is 0.393MPa. It involves an equipment hatch, several penetrations and liner with T-anchors. The pressurization process is achieved by supplying nitrogen to the test model up to containment failure.

This paper describes several techniques to obtain physically reasonable analysis results with better convergence and the summary of preliminary pre-test analysis using axisymmetric global modeling.

1. INTRODUCTION

Many techniques of treating post-cracking concrete behavior have been proposed for concrete structure analysis and the analysis modeling itself sometimes depends on the experiences. Although many seismic tests and analyses on reactor containment vessels have been conducted, few tests and analyses, focused on static internal pressure loading beyond design basis condition, have been conducted. As for reactor concrete containment Sizewell B in U.K.[1] and 1/6 scale reinforced concrete containment vessel (RCCV) test in U.S[2] were only available. Sizewell B was internal pressure loading test using 1/10 scale prestressed concrete containment vessel (PCCV) model, which was interrupted because of basemat uplift and could not reach ultimate structural condition. 1/6 RCCV test was conducted up to liner tearing and provided valuable data. However, it did not include the effect of prestressing of tendon.

Considering the above situation, NUPEC has been planning the ultimate strength test of 1/4 uniform scale PCCV imaging severe accident. The pre-test analysis will be compared with measured data and the post-test analysis using this test data will improve analysis model.

This paper describes several techniques to obtain physically reasonable analysis results with better convergence and the summary of preliminary pre-test analysis using axisymmetric global modeling..

2. COMPUTATIONAL MODELS

2.1 Material properties

The measured average data of concrete Young's modulus, Poisson's ratio, compressive strength, and tensile strength were used based on the trial mix concrete tests after field curing. As for rebars, the average stress-strain curves of each rebar material test were used except dumbbells. The average stress-strain curves obtained from the liner material tests were also used, assuming isotropy of the material. Two-dimensionality of liner material was considered by Mises yield function. The measured stress-strain curve of a tendon material test was used.

2.2 Material models

A finite element program ABAQUS/Standard Ver. 5.8 was used to predict the global behavior of 1/4 PCCV test. The stress-strain curve of post-cracking concrete was determined through the following sensitivity study, referring to the displacement data at the cylinder mid point of the 1/6 RCCV test results conducted at SNL.[1] That is, various tension-stiffening curves were adopted under full shear retention model. The tension-stiffening was assumed to be linearly decreased and was reduced to zero at strain values of 10, 20, 30, 40 and 50 times of the concrete crack strain of 1.28×10^{-4}, considering the simplicity of global analysis. The 10 times model

was the best agreement with 1/6 RCCV data. However this 10 times model induced unstable behavior above 3.0 times design pressure (Pd) condition so that 1 % crack stress was retained even after 10 times of the crack strain.

The reduction of the shear modulus after concrete cracking was determined as follows. The full shear retention model was compared with the model in which shear stiffness under cracking condition was reduced linearly to zero at 10 times of crack strain, similar to the above tension stiffening model. Both models were calculated up to 3.4 Pd where concrete cracking in hoop direction extended to the whole region. The analysis results were almost same so that the full shear retention model was adopted because of the better convergence of calculation.

Non-linear behavior in multi-axial stress field was traced by crack detection surface and compressive surface incorporated in ABAQUS code. Except for the measured ratio of the tensile strength to the compressive strength, defaults values of the surface parameters in ABAQUS were used because of no biaxial test data.

2.3 Modeling of 1/4 PCCV test facility

The axisymmetric global analysis was conducted as the first step pre-test analysis. The analytical model included general parts of a dome, a cylinder and a basemat, as shown in Fig. 1. The wall of dome part and cylinder part was divided into 6 elements to evaluate bending behavior. The dome part was divided into 45 elements and the cylinder part was divided into 60 elements. The basemat had 10 vertical elements and 42 radial elements. However, the juncture region between basemat and cylinder had finer elements. The model included the total numbers of 1963 nodes and 1279 elements.

In order to select an element type for the concrete, three solid element types were compared (4-node bilinear (ABAQUS:CAX4), 8-node biquadratic reduced integration (ABAQUS:CAX8R) and 4-node bilinear incompatible mode (ABAQUS:CAX4I)). When 8-node biquadratic reduced integration element and the 4-node bilinear incompatible mode element were used, very high stress occurred in the loading end at about 3.0 Pd and the calculation became divergent. It was supposed that the force directions of some nodes in a element was inconsistent with the direction of element stress in these cases. Since the materials exhibited strong non-linearity and the contact between tendon and concrete was important under high internal pressure condition, 4-node bilinear element was adopted.

Rebar was defined as reinforcement (ABAQUS:REBAR) in solid element. Liner was modeled by shell element (ABAQUS:SAX1) and the liner node was commonly shared with inside node of concrete.

2.4 Analytical modeling

Hoop tendon was modeled by rebar bonded to the concrete. Meridional tendon was modeled by shell element and the hoop direction stiffness was made zero in the cylinder part. The hoop direction stiffness was considered only above 45° dome angle, because the meridional tendons in the dome part are arranged as like mesh. Friction was specified between the concrete and the meridional tendon. The meridional tendon was allowed to slide relative to the concrete. Friction coefficient at dome part was 0.2156 which consisted of μ=0.21, average value of the measured friction coefficient, and friction coefficient considering tendon length effect (λ=0.001 per unit length). For cylinder part, μ=0 and λ=0.001 were used to stabilize the analysis. Although an empirical friction correlation between tendon and sheath was proposed as a function of loading end load and circumferencial angle,[3] it was not used for the present global axisymmetric analysis. Because hoop tendons don't have a tensile force distribution and meridional tendons are arranged as like mesh.

As a boundary condition, a horizontal direction was fixed along axisymmetric axis to realize axisymmetric condition. Non-linear soil springs were placed at the bottom of basemat to simulate the ground reaction force. The actual ground stiffness was used against compression force and it was zero against tension force. However, the soil springs in non-uplift part had stiffness against tension force, because the vertical displacement became too large when all tensile stiffness of soil springs in non-uplift part were zero. The gravity was considered only at the bottom of basemat as a concentrated force. That is, gravitational force at each node was neglected because of quite smaller force compared with tendon tensile force.

In order to simulate a setting loss condition of tendon, meridional tendon was prestressed with the prescribed value of 503 kN and then loosed to the prescribed value of 470 kN. As for hoop tendon initial stress of 991 MPa, corresponding to the average value of hoop tendon stress, was imposed.

3. SENSITIVITY STUDIES FOR THE DETERMINATION OF ANALYTICAL MODELINGS

This section describes the analytical techniques to obtain appropriate analysis results. The main techniques are treatments of dome part meridional tendon, consideration of soil spring and treatment of gravity.

3.1 Treatment of dome part meridional tendon

Two modelings of meridional tendon in dome part were compred. The one model simulated hoop stiffness in the meridional tendon above 45° dome angle (model (a)), and the other model simulated hoop stiffness in the meridional tendon above spring line (model (b)). The difference of two models was observed from 2.3 Pd. The apex displacement of model (a) increased in downward direction, while in model (b) it increased in upward direction.

The difference of displacement for two models depended on cracking condition in hoop direction. The difference of cracking condition for the two models became remarkable at 2.4 Pd. In model (a) cracking extended to dome part, while in model (b) it occurred in the cylinder part only.

As mentioned above, the vertical displacement depended on tendon modeling in the dome part. However, the test model failure will occur near penetrations in the middle cylinder part and the strain distribution of the cylinder part for both models were same. The model (a) was finally selected in the present analysis because of the better convergence under higher internal pressure.

3.2 Consideration of soil spring

Ground stiffness affects the global deformation behavior via ground reaction force under high internal pressure condition. Therefore, the reaction force of the ground was taken into account by placing soil springs at each node of basemat. The uniform soil spring stiffness values of $1x10^{12}$ N/mm, $1x10^{6}$ N/mm, $1x10^{4}$ N/mm and $1x10^{2}$ N/mm were used for sensitivity analysis. As a result, it was found that soil spring stiffness affected not only deformation behavior but also the convergence under high internal pressure condition. The difference of analysis results under high pressure condition was governed by the uplift condition of the basemat. The stiffness values of $1x10^{6}$ N/mm provided the best convergence which was consistent with the ground stiffness of actual test site of 30 MPa[4]. Therefore, the value of soil spring stiffness was finally distributed in proportion to the node area on the bottom of basemat which provided 30 MPa ground stiffness at each node.

3.3 Treatment of gravity

Gravitational force should be considered correctly to evaluate uplift behavior of the model, since actual soil spring of 30 MPa was adopted. Two models were compared. In one case, gravity was considered as concentrated mass at each Gaussian point as usual and in the other case, gravity was considered only at the bottom of the basemat as concentrated force.

Both analysis results were almost same, because vertical force by gravity was negligible compared with tendon tension force. For example, force balance of two elements at the apex of dome was evaluated as follows. Vertical component of the tensile force of meridional tendon was 25 kN. On the other hand, the vertical force by gravity was 0.49 kN, which was only 2 % compared with meridional tendon vertical force. Therefore, the gravity was considered only at the bottom of basemat as concentrated force.

In the ABAQUS model gravity is usually considered as concentrated mass at each Gaussian point and the displacement is calculated by solving equation of motion. Hence, calculation time was longer and the convergence of calculation became worse under large displacement condition.

4. ANALYSIS RESULTS

4.1 Structural behavior of 1/4 PCCV model

(1) Global deformation behavior

Figure 2 shows global deformation behavior for various internal pressures. A slight inward deformation was observed under setting condition due to the influence of prestressing. The cylinder part shape under 1.5 Pd became almost same as that before prestressing. The dome part deformed inward slightly under this pressure. The mid cylinder part begun to deform in outward direction at 2.2 Pd, while the dome part was compressive condition. Outward deformation of the mid cylinder part became remarkable at 3.6 Pd so that the dome part deformed downwards.

(2) Local displacement behavior

Figure 3 shows radial displacements versus pressure at various locations. The largest displacement was analyzed at slightly upper region (No. 4) from the mid plane of cylinder part. This was because the constraint force at basemat was larger than that at dome part. The region near the basemat (No. 5) and the dome (No. 2) part had small displacement. The displacements in the cylinder part (No. 3), (No. 4) increased linearly until about 2.1 Pd,

in which concrete cracking occurred in hoop direction as described below. They increased drastically at about 3.5 Pd due to the concrete cracking in meridional direction.

Figure 4 shows vertical displacements versus pressure at various locations. The apex (No. 1) had maximum downward deformation at setting condition due to the existence of mesh-like meridional tendon. Downward displacement of the apex decreased linearly up to about 2.4 Pd and it increased from about 2.4 Pd. However, it deceased from 3.6 Pd again, since vertical concrete cracking crack extended to the whole cylinder part. The displacement at 45° point from spring line (No. 2) had also downward deformation. It was smaller than the displacement at the apex. The displacement at mid part of cylinder part (No. 4) and spring line (No. 3) gradually increased until about 3.2 Pd and increased drastically from 3.5 Pd. The displacement near basemat (No. 5) deformation remained small.

(3) Concrete cracking behavior

Figure 5 shows concrete cracking behavior in both hoop and meridional directions. Hoop cracking initially occurred at 2.1 Pd (Fig. 5(a)-2). The hoop cracking caused the non-linear radial displacement as shown in Fig. 3. The hoop cracking extended above spring line at 2.4 Pd (Fig. 5(b)-2). Since the dome part constraint force was large, linear vertical deformation of cylinder part was maintained up to about 2.4 Pd as shown in Fig. 4. The cylinder part deformed outward slightly as shown in Fig. 2(c). Although outer surface cracking in the meridional direction extended to cylinder part at 3.4 Pd, there was no inner surface cracking as shown in Fig. 5(c)-1. Both hoop and meridional cracking almost extended to the whole region at 3.6 Pd (Fig. 5(d)), under which radial displacement increased drastically as shown in Fig. 5. Concrete stiffness became almost zero in both hoop and meridional directions at 3.6 Pd. Hence, vertical displacement in dome part changed from downward direction to upward direction as shown in Fig. 4. Bending behavior was observed in the meridional direction so that meridional cracking mainly occurred outside of concrete wall as shown in Fig. 5(d)-1.

(4) Strain distribution

Figure 6 shows hoop liner strains versus pressure at various locations. Hoop liner strain remained negative until about 1.5 Pd due to the tensile force of tendon. The liner strain of mid part (No. 4) of cylinder increased non-linearly from about 2.1 Pd and it increased drastically at about 3.5 Pd. These were closely related to the concrete cracking condition in the hoop direction at 2.1 Pd as shown in Fig. 5(a)-2 and concrete cracking in meridional direction at 3.6 Pd as shown in Fig. 5(d)-1. Although similar strain behavior occurred at spring line (No. 3) and dome part (No. 2), the strain level was lower than that in mid part of cylinder. The strain near basemat (No. 5) was almost zero because of the strong constraint force of the basemat. The hoop stiffness of concrete became almost zero at 3.4 Pd and the rebar in cylinder part was almost yielded at this pressure (yield stress : 459 MPa). That is, the change in liner strain was explained by the changes in concrete and rebar stiffness.

Figure 7 shows the meridional liner strain versus pressure at various locations. The meridional strain near basemat (No. 5) was increased non-linearly from about 2.0 Pd due to the initiation of ballooning of cylinder part as shown in Fig. 2 (c). On the other hand, the strains of other locations were very small up to 3.4 Pd due to the lack of inner surface concrete cracking in meridional direction as shown in Fig. 5(c)-1. The strain of spring line (No. 3) increased drastically from 3.4 Pd, because the spring line deformed outwards remarkably as shown in Fig. 3 and the dome part was tensiled in both hoop and meridional directions. As a result, the strain was concentrated at spring line where structure was discontinuous.

Figure 8 shows the hoop strains of tendon. It exhibited similar behavior as liner strain if the initial prestressing strain condition was considered.

2.3.2 Summary of global analysis

Figure 9 shows the distribution relationship of hoop stress of outside concrete, hoop stress of outside rebar and hoop stress of tendon, in contrast with the cracked region in hoop direction and the overall deformation for several values of Pd.

The stress of tendon and outside rebar were almost uniform under 2.0 Pd condition as shown in Fig. 9(a). Because internal pressure was imposed equally on the inner surface of containment and hoop rebar and hoop tendon were not constrained by the vertical force under low pressure condition. The stress of concrete was nearly uniform in the cylinder part except near basemat and spring line, since the constraint forces of dome part and basemat governed the local displacement. The concrete stress decreased along the top of the dome and increased slightly in the apex region. Since hoop stress was proportional to the radius, the membrane stress should reduce to

zero at the apex. However, outside stress increased slightly at the apex region because of the occurrence of bending behavior in the apex region.

Concrete crack initiated at 2.4 Pd, thereby the stress of concrete in the cylinder part decreased as shown in Fig. 9(b). As a result, the stress of rebar and tendon increased remarkably. This clearly demonstrated the role of prestressed concrete, in that the decreasing stress of concrete was supplemented by rebars and tendons.

The stress of concrete became almost zero and the stress of rebar became nearly uniform because of the yielding at 3.7 Pd as shown in Fig. 9(c). The stress of tendon also became nearly uniform in the cylinder part because of the yielding. Hence the displacement increased in the radial direction remarkably.

In summery, concrete cracking governed the global behavior of PCCV. That is, the reduction of concrete stress due to cracking caused the changes in stress distribution of rebars and tendons and resultant global deformation behavior.

ACKNOWLEDGMENTS

This work is sponsored under the contract by the Ministry of International Trade and Industry, Japan.

REFERENCES

(1) Twidale, D., and Crowder R., 1991, "Sizewell 'B' - a One Tenth Scale Containment Model Test for the UK Programme," Nuclear Engineering and Design 125 85-93

(2) Horschel, D. S., 1992, "Experimental Results from Pressure Testing A 1:6-Scale Nuclear Power Plant Containment," NUREG/CR-5121, SAND88-0906

(3) Kashiwase, T., and Nagasaka, H., 1997, " Analysis Study on Change of Tendon Tension Force Distribution during the Pressurization Process of Pre-stressed Concrete Containment Vessel, " Proceedings of ICONE-5

(4) Miller, C. M., 1992, "Geotechnical Investigation job No. 1-20904 Containment Technology Test Facility - west Albuquerque, New Mexico," GEO-TEST

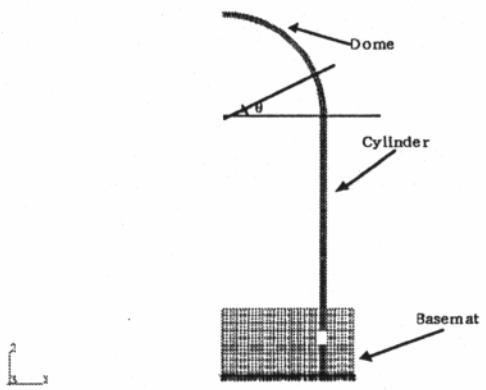

Fig. 1 Axisymmetric global analysis modeling

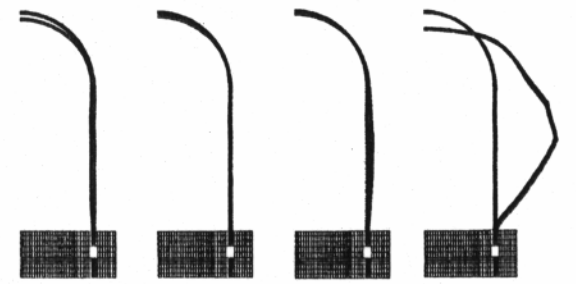

(a) Setting (b) 1.5 Pd (c) 2.2 Pd (d) 3.6 Pd

Fig. 2 Deformation of test vessel for various internal pressures

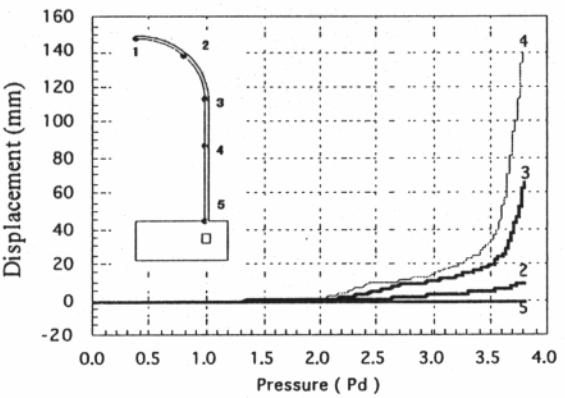

Fig. 3 Radial displacements at various locations

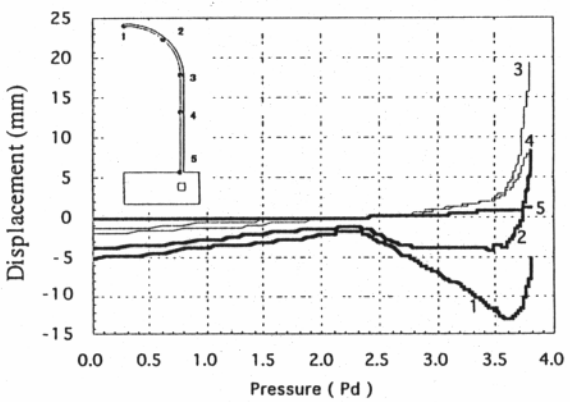

Fig. 4 Vertical displacements at various locations

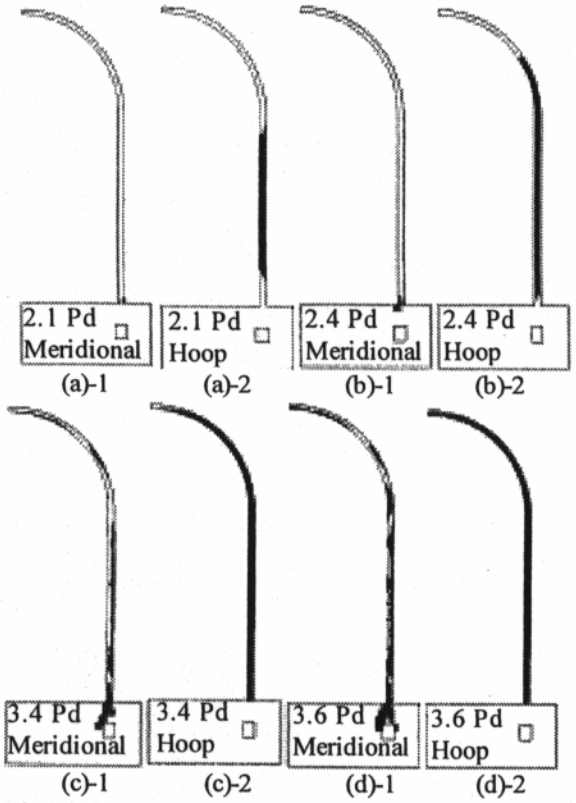

Fig. 5 Concrete cracking behavior in both hoop and meridional directions

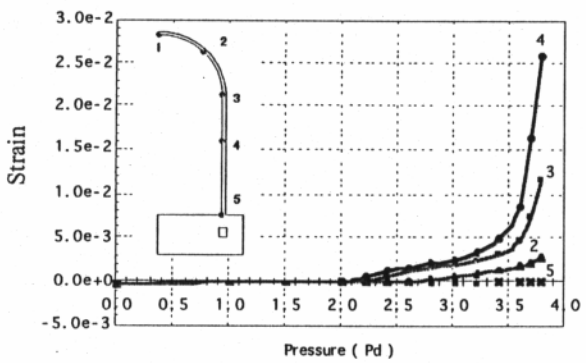

Fig. 6 Hoop liner strains at various locations

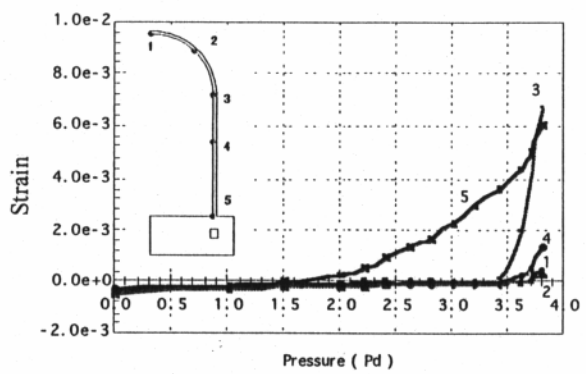

Fig. 7 Meridional liner strains at various locations

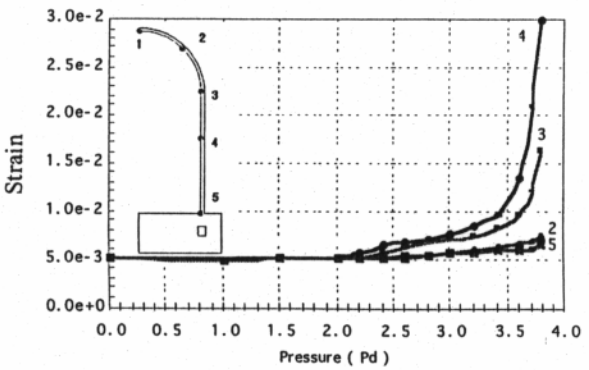

Fig. 8 Hoop tendon strains at various locations

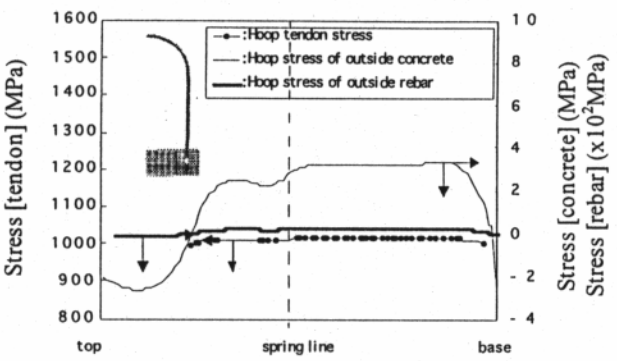

(a) 2.0 Pd

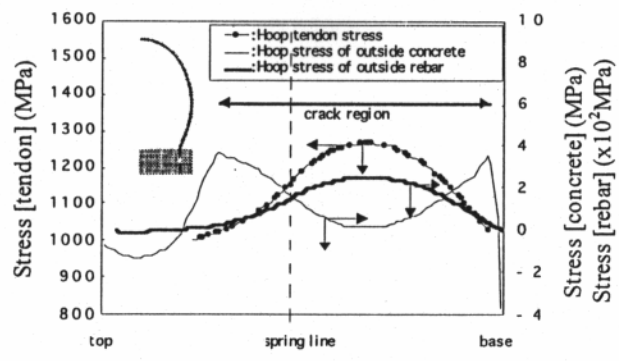

(b) 2.4 Pd

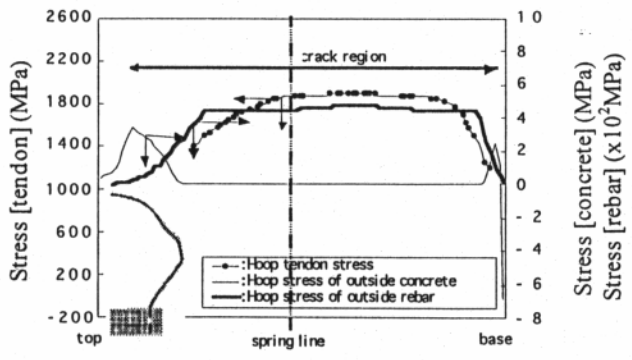

(c) 3.7 Pd

Fig. 9 Relation of several stresses at various internal pressures